CHEMISTRY OF MATERIALS
Article

Chem. Mater. **2009,** *21,* 4425–4433 4425
DOI:10.1021/cm900982a

Simultaneous Optimization of Light Gain and Charge Transport in Ambipolar Light-Emitting Polymer Field-Effect Transistors

Michael C. Gwinner,[†] Saghar Khodabakhsh,[†] Harald Giessen,[‡] and Henning Sirringhaus*[,†]

[†]*Cavendish Laboratory, J. J. Thomson Avenue, Cambridge CB3 0HE, United Kingdom, and*
[‡]*4. Physikalisches Institut, Universität Stuttgart, Pfaffenwaldring 57, 70569 Stuttgart, Germany*

Received April 9, 2009. Revised Manuscript Received July 23, 2009

Ambipolar light-emitting field-effect transistors (LEFETs) based on poly(9,9-dioctylfluorene-*alt*-benzothiadiazole) (F8BT) are able to combine electrical switching capability with the generation of light within a well-defined recombination zone inside the channel. Therefore, they are an attractive architecture not only for low-loss light signal transmission in optoelectronic integrated circuits but also for the potential realization of electrically pumped organic lasers. However, these applications require a simultaneous optimization of transistor performance and waveguiding of emitted light. Here we show that to achieve efficient waveguiding and optical gain the annealing temperature of the F8BT film has to be kept at 120 °C below its glass transition temperature. At such low processing temperatures it is difficult to achieve efficient ambipolar charge injection from gold source/drain electrodes and charge transport at the active transistor interface. We show that modification of the gold electrodes with a 1-decanethiol self-assembled monolayer (SAM) allows efficient charge injection into F8BT films deposited on top. The performance of such ambipolar LEFETs with SAM-modified electrodes is better than that of devices with bare gold electrodes but processed at higher temperatures.

Introduction

As a result of their unique properties, semiconducting conjugated polymers have gained enormous interest in recent years.[1−4] An ambipolar field-effect transistor based on these materials[5−7] constitutes a powerful optoelectronic device, which combines electrical switching capability with the generation of light within a well-defined recombination zone inside the channel. In such a light-emitting field-effect transistor (LEFET) both electron and hole accumulation layers can be simultaneously formed within the channel.[8] Where the two layers meet, charge recombination occurs, and thus light emission is observed. As high current densities can be obtained[9] and the light emission can be chosen to occur far away from absorbing metal electrodes, LEFETs are a versatile and attractive architecture not only for low-loss light signal transmission in optoelectronic integrated circuits but also for the realization of electrically pumped organic lasers.[10−13] The intention of using an LEFET based on the polymer poly(9,9-dioctylfluorene-*alt*-benzothiadiazole) (F8BT) for these applications requires simultaneous device optimization of transistor performance and waveguiding of the emitted light. In this paper it is demonstrated that substantial modifications to the device processing have to be made to achieve such simultaneous optimization of the optical and electronic properties. Of crucial importance is the F8BT postdeposition annealing after the spin-coating, which influences both the ambipolar transistor current and thus light emission intensities, as well as the amplified spontaneous emission (ASE) behavior, which represents a figure of merit for efficient waveguiding and gain. In our previous work on F8BT ambipolar LEFETs we found that high annealing temperatures above the liquid crystalline melting temperature of F8BT had to be used to obtain the best transistor performance.[7,9,14] The reasons why such high annealing temperatures were required were not well understood. Unfortunately, we find that this annealing step is not compatible with waveguiding and lasing applications.

*Corresponding author. E-mail: hs220@cam.ac.uk.

(1) Burroughes, J. H.; Bradley, D. D. C.; Brown, A. R.; Marks, R. N.; Mackay, K.; Friend, R. H.; Burns, P. L.; Holmes, A. B. *Nature* **1990**, *347*, 539.
(2) Holzer, W.; Penzkofer, A.; Gong, S.-H.; Bleyer, A.; Bradley, D. D. C. *Adv. Mater.* **1996**, *8*, 974.
(3) Friend, R. H.; Gymer, R. W.; Holmes, A. B.; Burroughes, J. H.; Marks, R. N.; Taliani, C.; Bradley, D. D. C.; Santos, D. A. D.; Bredas, J. L.; Logdlund, M.; Salaneck, W. R. *Nature* **1999**, *397*, 121.
(4) McGehee, M. D.; Heeger, A. J. *Adv. Mater.* **2000**, *12*, 1655.
(5) Swensen, J. S.; Soci, C.; Heeger, A. J. *Appl. Phys. Lett.* **2005**, *87*, 253511.
(6) Zaumseil, J.; Friend, R. H.; Sirringhaus, H. *Nat. Mater.* **2006**, *5*, 69.
(7) Zaumseil, J.; Donley, C. L.; Kim, J.-S.; Friend, R. H.; Sirringhaus, H. *Adv. Mater.* **2006**, *18*, 2708.
(8) Zaumseil, J.; Sirringhaus, H. *Chem. Rev.* **2007**, *107*, 1296.
(9) Naber, R. C. G.; Bird, M.; Sirringhaus, H. *Appl. Phys. Lett.* **2008**, *93*, 023301.
(10) Muccini, M. *Nat. Mater.* **2006**, *5*, 605.
(11) Nakanotani, H.; Akiyama, S.; Ohnishi, D.; Moriwake, M.; Yahiro, M.; Yoshihara, T.; Tobita, S.; Adachi, C. *Adv. Funct. Mater.* **2007**, *17*, 2328.
(12) Namdas, E. B.; Tong, M.; Ledochowitsch, P.; Mednick, S. R.; Yuen, J. D.; Moses, D.; Heeger, A. J. *Adv. Mater.* **2008**, *20*, 1.
(13) Gwinner, M. C.; Khodabakhsh, S.; Song, M. H.; Schweizer, H.; Giessen, H.; Sirringhaus, H. *Adv. Funct. Mater.* **2009**, *19*, 1360.
(14) Schidleja, M.; Melzer, C.; von Seggern, H. *Adv. Mater.* **2009**, *21*, 1.

Published on Web 09/04/2009

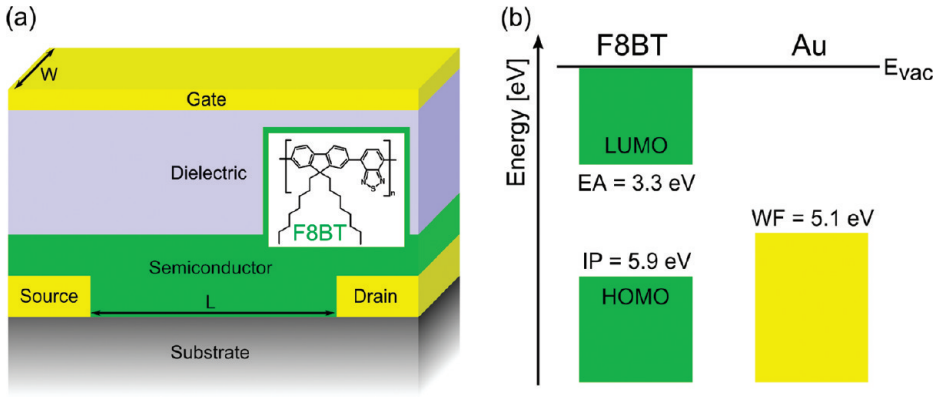

Figure 1. (a) Schematic illustration of the top gate/bottom contact organic field-effect transistor structure. (b) Visualization of the highest occupied molecular orbital (HOMO) and lowest unoccupied molecular orbital (LUMO) levels of F8BT in relation to the workfunction (WF) of gold.

We demonstrate here how the modification of the injecting electrodes with self-assembled monolayers (SAMs), in particular 1-decanethiol, allows for the use of low annealing temperatures below the F8BT glass transition, and therefore the coincident optimization of the different properties required for these optoelectronic devices.

Experimental Section

Materials. All materials were used as purchased without further purification. F8BT with medium molecular weight (M_n = 100 kg mol^{-1}, polydispersity 2.08) received from Cambridge Display Technologies Ltd. served as semiconductor. PMMA (M_n = 350 kg mol^{-1}, Polymer Source Inc.) was used as dielectric. All applied SAMs were supplied by Sigma Aldrich in liquid form.

Fabrication. Low alkali glass (0.7 mm thick, Präzisions Glas & Optik GmbH) served as substrate for all structures. Apart from the organics, all materials were thermally evaporated. In case of LEFETs, the source/drain gold electrodes (30 nm, oxygen plasma treated) were patterned via photolithography and a double-layer lift-off process. A thin layer of chromium (0.7 nm) provided improved adhesion of the gold. When indicated, a specific SAM was then deposited onto the injecting gold electrodes by placing the samples into a 5 mM solution in pure ethanol for more than 12 h. Whereas F8BT was subsequently spin-coated using anhydrous xylene as solvent, the use of anhydrous *n*-butylacetate for the PMMA deposition allowed spinning on top of the F8BT films without intermixing. Solution concentrations and spin speeds were adjusted to give the desired thicknesses. Evaporating a thin gate electrode through a shadow mask completed the LEFET structure. All processing steps after the electrode patterning were carried out in a dry nitrogen glovebox.

Characterization. Transistors were characterized in a dry nitrogen glovebox with an Agilent 4155B semiconductor parameter analyzer. The emitted light intensity was measured with a silicon photodiode (Hamamatsu, S1133-01), which is mounted directly above the device and has a sensitivity of 0.3 A W^{-1} at around $\lambda = 560$ nm. Optical excitation was performed in ambient atmosphere with a TOPAS (Light Conversion Ltd.) laser system (λ = 486 nm, pulse width $\sim$ 100 fs, repetition rate 1 kHz). An Ocean Optics USB2000 spectrometer recorded induced PL spectra. Electrode workfunctions were detected with a Kelvin Probe System by Besocke Delta Phi GmbH (Jülich, Germany). Contact angle measurements were performed with a DSA-100 system by Krüss GmbH (Hamburg, Germany).

Results and Discussion

1. Influence of F8BT Annealing Temperature. The fabricated ambipolar LEFET structure consists of a top gate/bottom contact architecture with the F8BT active layer on top of injecting gold source/drain electrodes. The semiconductor film is isolated from the semitransparent gate electrode, consisting of either gold or silver, by a poly(methyl methacrylate) (PMMA) gate dielectric. Figure 1a illustrates the device structure, whereas Figure 1b contains a schematic of the energy levels for charge injection. We first investigated the influence of the F8BT annealing after spin-coating on the transistor performance in our standard LEFET architecture with bare gold source/drain electrodes. The annealing temperature was varied from 120 to 290 °C and applied for 20 min before quenching the samples on a metal plate. The F8BT thickness is relatively thick (70−75 nm) to exceed the waveguide cutoff thickness, to increase the mode confinement within the polymer semiconductor,[15] and to improve the isolation of the mode confined in the polymer semiconductor from the absorbing gate electrode which is separated from the polymer semiconductor by a PMMA buffer layer that cannot be made too thick because it needs to act as an effective gate dielectric. The choice of F8BT thickness is the result of a careful optimization based on mode simulations.[13] However, in our top gate/bottom contact device structure charges need to be transported from the electrodes through the bulk of the film, and for such thick films contact resistance, particularly for electron injection into the channel, becomes significant.[16,17] After the PMMA spin-coating a further annealing step at 120 °C for 60 min is performed for all samples to remove residual solvents and moisture.

It is found that annealing at high temperatures, ideally at 290 °C, significantly improves the ambipolar transistor performance by reducing threshold voltages and hysteresis. This is particularly important for strong light emission since a wider voltage range for ambipolar operation is possible. Figure 2a shows a comparison of the transistor

(15) Yarif, A.; Yeh, P. *Optical Waves in Crystals*; Wiley: New York, 2003.
(16) Bürgi, L.; Richards, T. J.; Friend, R. H.; Sirringhaus, H. *J. Appl. Phys.* **2003**, *94*, 6129.
(17) Richards, T. J.; Sirringhaus, H. *J. Appl. Phys.* **2007**, *102*, 094510.

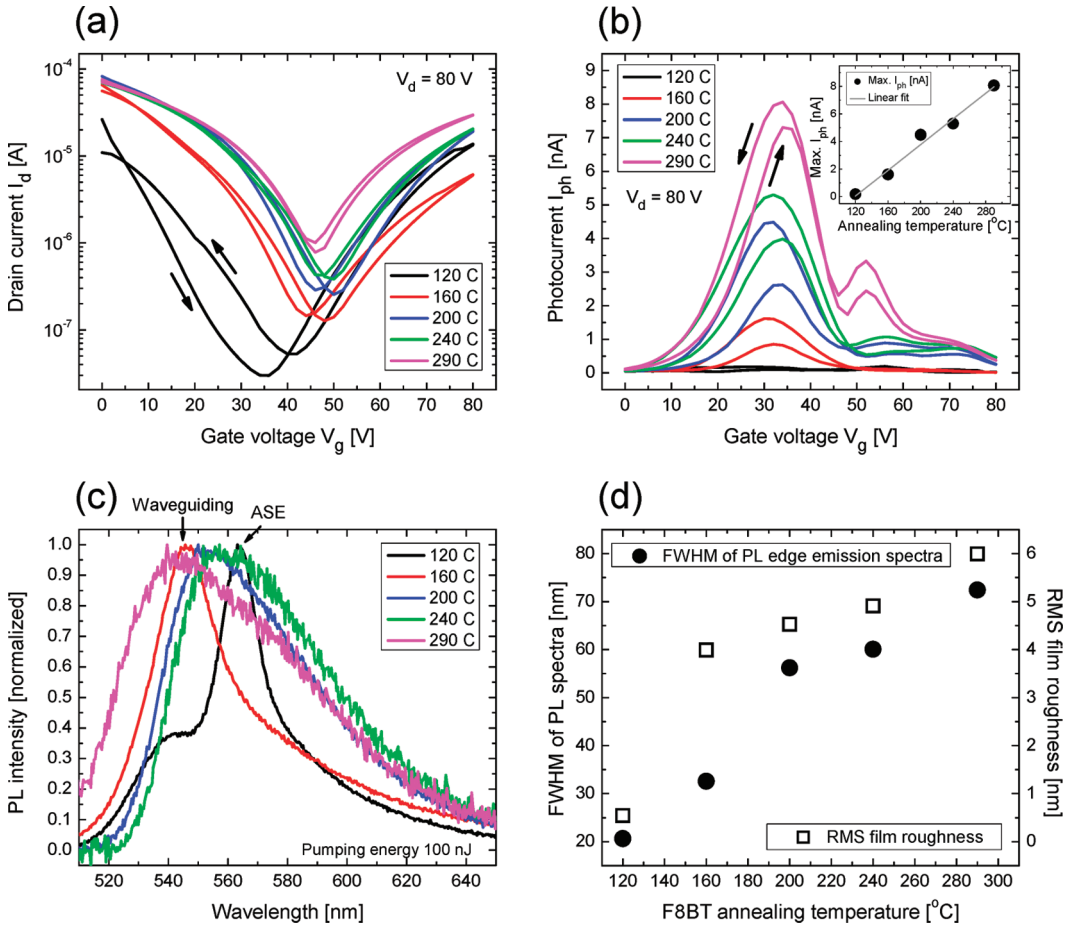

Figure 2. (a) Comparison of the LEFET (L = 10 μm, W = 4 cm, 70 nm F8BT, 325 nm PMMA, 15 nm Au gate) transfer characteristics for F8BT annealing temperatures between 120 and 290 °C. (b) Corresponding photocurrents during the transfer sweeps. The inset shows the respective maximum photocurrents. (c) Comparison of the PL spectra at the sample edges of 155 nm thick F8BT films annealed at temperatures between 120 and 290 °C while being excited with an energy of 100 nJ. (d) Corresponding fwhm of the spectra and rms film roughness.

currents I_d during a transfer scan. The transistors with F8BT processed at 290 °C show best performance, whereas reduced annealing temperatures yield lower transistor currents for both electrons and holes. In the ambipolar operation regime, which is the region in the transfer scan around the gate voltage at which the current is at a minimum, the current is already more than halved for 240 °C. It further drops to 15% and only 4% for annealing temperatures of 160 and 120 °C, respectively. Moreover, the hysteresis between forward and backward scan becomes systematically more pronounced for reduced annealing temperature, which is attributed to charge trapping during electron accumulation and subsequent detrapping during hole accumulation and vice versa. The ambipolar current suppression exhibits a severe effect on the accompanied electroluminescence intensity in this regime, quantified by the photocurrent measured by a photodiode above the LEFET top surface. The plot of the corresponding photocurrents I_{ph} in Figure 2b shows that the maximum light intensity drops approximately linearly by 2 orders of magnitude between the two extreme annealing temperatures.

Analyzing the transfer curves in terms of mobilities μ and threshold voltages V_{th} for holes and electrons gives further insight into the performance problems occurring for lower annealing temperatures. A detailed plot of the results can be found in the Supporting Information (Figure S1). To avoid artifacts due to the hysteresis, the parameter fitting of the carrier mobilities μ and the threshold voltages V_{th} is performed in the unipolar regimes, in which the device is driven from depletion into accumulation. The equations for the drain current I_d in the respective saturation regime as a function of the gate voltage V_g and the drain voltage V_d are given by

$$I_d = \frac{WC_i}{2L}\mu_e(V_g - V_{th,e})^2 \quad \text{for electrons} \qquad (1)$$

$$I_d = \frac{WC_i}{2L}\mu_h(V_d - (V_g - V_{th,h}))^2 \quad \text{for holes} \qquad (2)$$

Here, W and L represent the channel width and length, and $C_i = \varepsilon\varepsilon_0 t^{-1}$ is the capacitance per area of the PMMA with dielectric constant ε = 3.6 and thickness t.

For 120 °C the hole mobility is less than half of the constant value for the higher temperatures, dropping from 1.5 × 10^{-3} cm^2 V^{-1} s^{-1} to 7 × 10^{-4} cm^2 V^{-1} s^{-1}. The hole threshold voltage increases from a constant value of around −30 V to −40 V above 120 °C to

more than −50 V for 120 °C. A similar trend can be observed for the electron threshold. It exhibits a minimum of around 40 V for 290 °C, whereas it is larger for all lower temperatures (46−48 V). The electron mobilities show a more complicated temperature behavior. The electron mobility is relatively insensitive to annealing temperature in the temperature range between 200 and 290 °C with a value of 1×10^{-3} cm^2 V^{-1} s^{-1}. It is then reduced to 3×10^{-4} cm^2 V^{-1} s^{-1} near T_g at 160 °C. Further reducing the annealing temperature below the glass transition temperature to 120 °C, however, appears to yield an increased electron mobility of 7×10^{-4} cm^2 V^{-1} s^{-1}.

The general trend of increased electron and hole threshold voltages with increased annealing temperature is primarily responsible for the reduction of the current in the ambipolar regime. Two main factors should be considered to explain this dependence on threshold voltage on annealing temperature. The annealing might either reduce the concentration of charge traps or generally improve the electronic properties at the active semiconductor dielectric interface in the channel, or it might improve the contact between the metal source/drain electrodes and the polymer, and thus reduce contact resistance. We will argue below that the high threshold values are mainly due to a poor contact of the F8BT to the gold electrodes.

The decrease of the electron mobility from 120 to 160 °C can be explained by conformational changes of the F8BT chain stacking below and above the glass transition temperature. Between 120 and 160 °C a rearrangement of the F8BT chains occurs into an energetically more favorable packing structure, which exhibits less overlap between BT units of neighboring polymer chains, making the electron hopping transport between those sites less favorable.[18] Hole transport, on the other hand, is more delocalized along the polymer backbone and is less affected by this conformational change. For holes the dependence of the mobility on annealing is therefore entirely determined by the elimination of charge traps and/or the improvement of contact resistance.

Apart from their consequences on the transistor currents, processing conditions for polymer LEFET acting laser light source or low-loss optical signal transmitter have to be optimized for efficient waveguiding to ensure large traveling distances of the emitted light through the active region. In this regard, ASE characteristics of F8BT films annealed at temperatures between 120 and 290 °C are investigated. A slab waveguide structure with 155 nm F8BT spun on top of the glass substrate is fabricated to exceed the cutoff value for the transversal electric (TE) ground-mode.[15] A focused laser spot is pumping the F8BT from the top and positioned in the vicinity of the edge, pumping a region with the length of the spot diameter. Subsequently, the induced light emission from the edge, resulting from photons traveling alongside the length of the pump region toward the edge, is detected with an optical fiber. Figure 2c shows the normalized spectra for the different F8BT films excited with a pump energy of 100 nJ. For F8BT films annealed at only 120 °C, the photoluminescence (PL) spectrum collapses into an ASE peak centered at 563 nm, implying that the emitted light is amplified efficiently as it travels alongside the laser spot width toward the edge.[19,20] For higher annealing temperatures, however, ASE behavior cannot be observed, even for larger pump energies. Instead, the spectra only show a slightly modified PL of F8BT with peak around 550 nm and decreasing intensity for higher temperatures. Despite severe waveguiding losses, a certain spectral narrowing can be observed when the annealing temperature is decreased from 290 °C down to 160 °C. The full width at half-maximum (fwhm) of the individual spectra can be utilized to quantify the waveguiding efficiency of the individual films. From Figure 2d it becomes obvious that the ASE peak for 120 °C has the smallest fwhm value by far (20 nm). Decent waveguiding can still be obtained for 160 °C, although the fwhm value of 32 nm is likely to overestimate the waveguiding ability as the spectrum does not show ASE. For higher temperatures, the fwhm steadily increases, indicating major losses and poor waveguiding. These results show that to achieve good ASE/lasing characteristics the F8BT films cannot be annealed at more than 120 °C. The detailed ASE results of the film annealed at 120 °C are available in the Supporting Information (Figure S2). An ASE threshold energy of about 60 nJ is extracted. The wavelength of 563 nm indicates the one of minimal loss for given material gain spectrum.[21]

To explain the observations regarding the transistor and ASE performance we need to take into account the impact of the annealing temperature on the morphology of the F8BT film. Morphological changes as a function of annealing temperature have been investigated by atomic force microscopy (AFM) and optical microscopy (Figure 3). The AFM image of the film annealed at 120 °C reveals an amorphous F8BT phase and a very flat surface with a root-mean-square (rms) roughness of about 0.5 nm. Annealing at temperatures between 160 and 200 °C does not change the morphology qualitatively. The rms roughness, however, increases by an order of magnitude averaging 4.0 nm for 160 °C and 4.5 nm for 200 °C. This is possibly an indication of formation of a polycrystalline phase during annealing above T_g with yet very small grain size. A polycrystalline morphology with much larger domain size is apparent when the F8BT is annealed at 240 °C and beyond. The rms roughness increases

(18) Donley, C. L.; Zaumseil, J.; Andreasen, J. W.; Nielsen, M. M.; Sirringhaus, H.; Friend, R. H.; Kim, J.-S. *J. Am. Chem. Soc.* **2005**, *127*, 12890.

(19) McGehee, M. D.; Gupta, R.; Veenstra, S.; Miller, E. K.; Diaz-Garcia, M. A.; Heeger, A. J. *Phys. Rev. B* **1998**, *58*, 7035.

(20) Xia, R.; Heliotis, G.; Hou, Y.; Bradley, D. D. C. *Org. Electron.* **2003**, *4*, 165.

(21) Stevens, M. A.; Silva, C.; Russell, D. M.; Friend, R. H. *Phys. Rev. B* **2001**, *63*, 165213.

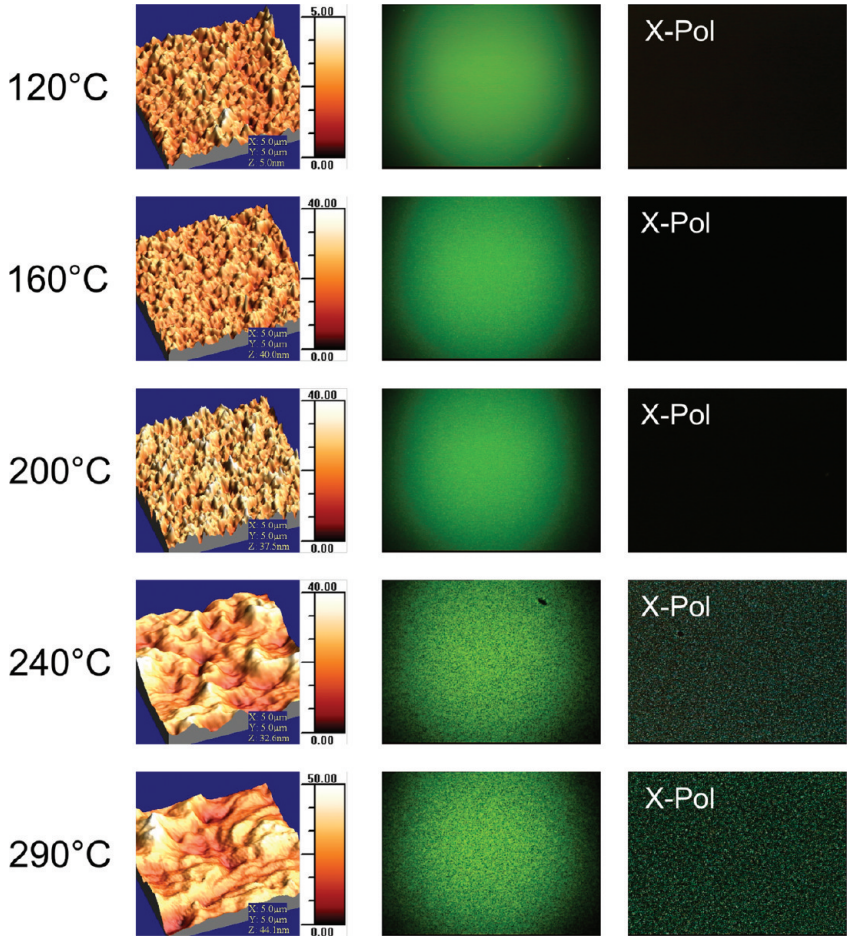

Figure 3. Comparison of the F8BT film morphologies for different annealing temperatures. For each temperature an AFM image, an optical microscopy (50× magnification) image, and a microscope image of the transmission through two orthogonal polarizers (X-Pol) is shown.

further and constitutes 6.0 nm for annealing at 290 °C. Consistent with these observations are optical microscope images, also presented in Figure 3. The luminescence images show that annealing at 120 °C does not change the amorphous character of the pristine F8BT film as the image is completely featureless. For 160 °C and beyond, some speckle contrast appears indicating a rougher film surface. These features become more pronounced when the F8BT is annealed at 240 or 290 °C. The cross-polarized images indicate they are due to progressive crystallization and the formation of large grains. Individual ordered domains in a polycrystalline material give rise to local birefringence, leading to a finite amount of light passing through the perpendicular polarizers. These observations are in excellent agreement with the AFM measurements and previously performed X-ray diffraction studies on respective F8BT films showing evidence of a progressive increase of the degree of crystallinity upon annealing.[18] The increase of grain size for annealing temperatures above 200−240 °C is also consistent with previous differential scanning calorimetry (DSC) and optical microscopy studies of the phase behavior of F8BT [23] and has been attributed to the polymer entering into a liquid crystalline mesophase during annealing with much increased chain mobility. With these results, it is possible to verify the conclusion that the strong losses preventing efficient waveguiding and ASE in F8BT annealed at temperatures of more than 120 °C are caused by severe light scattering due to the enlarged roughness and induced grain boundaries. Similar observations of ASE quenching in other polycrystalline polyfluorene gain materials such as F8 have been made previously.[22] This interpretation for our F8BT films is strongly supported by the correlation between the fwhm of the edge emission spectra and the corresponding rms film roughness, plotted together in Figure 2d.

2. Transistor Performance Improvement with SAMs. The restriction to amorphous F8BT in LEFETs to support efficient waveguiding of the emitted light creates the necessity of improving the transistor performance to increase the deteriorated emission intensity. This is of particular importance since the relatively large thickness of the semiconducting polymer required for decent waveguiding and sufficient isolation from the electrodes makes contact resistance a serious problem.[17] An efficient way of

(22) Sims, M.; Zheng, K.; Campoy Quiles, M.; Xia, R.; Stavrinou, P. N.; Bradley, D. D. C.; Etchegoin, P. *J. Phys.: Condens. Matter* **2005**, *17*, 6307.

(23) Banach, M. J.; Friend, R. H.; Sirringhaus, H. *Macromolecules* **2003**, *36*, 2838.

Table 1. Summary of the Characteristics of the Different Applied SAM Types

SAM type	core group	WF change (to gold ref)	contact angle (deionized water)
1DT	aliphatic, insulating, longer	-0.6 ± 0.2 eV	$125 \pm 2°$
FDT	aliphatic, insulating, longer	$+0.8 \pm 0.2$ eV	$118 \pm 2°$
MOTP	aromatic, conjugated, shorter	-0.3 ± 0.2 eV	$58 \pm 2°$
FTP	aromatic, conjugated, shorter	$+0.5 \pm 0.2$ eV	$66 \pm 2°$

tuning the charge carrier injection and thus the transistor current is to modify the gold contacts with the help of a self-assembled monolayer (SAM).[24−34] In F8BT-based top gate/bottom contact LEFETs contact resistance is a limiting factor due to the energy level mismatch with the gold workfunction. However, even with improved injection barriers due to SAM-modified electrodes, the current suppression in the linear regime is still strongly pronounced. This is because the contact resistance is also very sensitive to the contact of the polymer at the electrode interface and the bulk resistance of the material.[17] Corresponding output characteristics of SAM-modified devices can be found in the Supporting Information (Figure S4). Figure 4 and Table 1 summarize the chemical structures and properties of the different applied SAMs 1-decanethiol (1DT), 1*H*,1*H*,2*H*,2*H*-perfluorodecanethiol (FDT), 4-methoxythiophenol (MOTP), and 4-fluorothiophenol (FTP). As the amorphous character of the F8BT is not affected by these SAMs, the devices are compatible with applications requiring low scattering losses.

The impact of the SAM modifications on the transistor performance is visualized by the transfer characteristics in Figure 5a. By fitting the graphs within the respective hole and electron transport saturation regimes in the direction where the device is driven from depletion into accumulation, mobilities μ and threshold voltages V_{th} can be extracted. It is revealed that both the extracted mobilities and threshold voltages are strongly dependent on SAM treatment, that is, affected by contact resistance.[30] Figure 5b,c presents the fitting results for hole and electron transport, respectively. It is found that the hole mobility of a reference device of about 1.43×10^{-3} cm^2 V^{-1} s^{-1} remains constant or is slightly enhanced for the two aromatic SAMs MOTP and FTP. Much more pronounced are the differences when aliphatic SAMs are

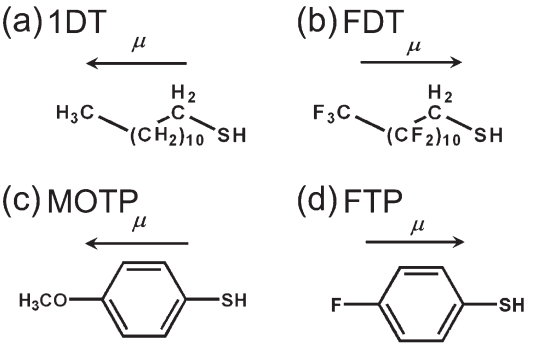

Figure 4. Chemical structures of the applied SAMs including the direction of their dipole moment μ: (a) 1-decanethiol (1DT), (b) 1*H*,1*H*,2*H*,2*H*-perfluorodecanethiol (FDT), (c) 4-methoxythiophenol (MOTP), and (d) 4-fluorothiophenol (FTP).

applied. As a result of their dipole moments pointing in opposite directions, 1DT shows a lower hole mobility than FDT, and the latter enhances the mobility substantially. Interestingly, the hole threshold voltage of the reference of −40 V is lowered considerably for all SAM-modified devices, whereby the longer aliphatic SAMs 1DT and FDT improve the threshold even further than the aromatic SAMs. However, the fact that the 1DT-modified device exhibits a more favorable value in comparison to the one with FDT is unexpected. The electron mobilities show the opposite behavior than the ones for holes. The reference value of about 7.6×10^{-4} cm^2 V^{-1} s^{-1} is enhanced by 1DT and MOTP. While FTP on the other hand moderately lowers the electron mobility, FDT halves the value. The electron threshold voltage of a reference device (58 V) remains unaltered for FTP. Yet, the other electron withdrawing SAM FDT increases the threshold voltage considerably. Also in the electron case, 1DT shows the smallest threshold voltage, considerably lower than the one with MOTP. As a result of the favorable electron and hole transport characteristics, the devices with 1DT showed the overall highest currents during an ambipolar IV-sweep, in which the gate is grounded and the voltage difference between source and drain is steadily increased. The comparison in Figure 5d shows that the current and, hence, the proportional light emission intensity are about a factor of 2 larger than for the other SAM-modified devices, and more than six times larger than for the unmodified device.

These results verify that the charge carrier injection is affected by the effective metal work function shift induced by the dipole moment of the SAM molecules (see Figure S3 in Supporting Information). The currents depend on the injection barrier with respect to the HOMO and LUMO of the F8BT. Therefore, SAMs with dipole moment pointing toward the F8BT such as 1DT and MOTP

(24) Campbell, I. H.; Kress, J. D.; Martin, R. L.; Smith, D. L.; Barashkov, N. N.; Ferraris, J. P. *Appl. Phys. Lett.* **1997**, *71*, 3528.
(25) Nüesch, F.; Si-Ahmed, L.; Francois, B.; Zuppiroli, L. *Adv. Mater.* **1997**, *9*, 222.
(26) Lin, Y.-Y.; Gundlach, D. J.; Nelson, S. F.; Jackson, T. N. *IEEE Trans. Electron Devices* **1997**, *18*, 1325.
(27) Khodabakhsh, S.; Poplavskyy, D.; Heutz, S.; Nelson, J.; Bradley, D. D. C.; Murata, H.; Jones, T. S. *Adv. Funct. Mater.* **2004**, *14*, 1204.
(28) de Boer, B.; Hadipour, A.; Mandoc, M. M.; Van Woudenbergh, T.; Blom, P. W. M. *Adv. Mater.* **2005**, *17*, 621.
(29) Khodabakhsh, S.; Sanderson, B. M.; Nelson, J.; Jones, T. S. *Adv. Funct. Mater.* **2006**, *16*, 95.
(30) Hamadani, B. H.; Corley, D. A.; Ciszek, J. W.; Tour, J. M.; Natelson, D. *Nano Lett.* **2006**, *6*, 1303.
(31) Asadi, K.; Gholamrezaie, F.; Smits, E. C. P.; Blom, P. W. M.; de Boer, B. *J. Mater. Chem.* **2007**, *17*, 1947.
(32) Stoliar, P.; Kshirsagar, R.; Massi, M.; Annibale, P.; Albonetti, C.; De Leeuw, D. M.; Biscarini, F. *J. Am. Chem. Soc.* **2007**, *129*, 6477.
(33) Marmont, P.; Battaglini, N.; Lang, P.; Horowitz, G.; Hwang, J.; Kahn, A.; Amato, C.; Calas, P. *Org. Electron.* **2008**, *9*, 419.
(34) Cai, Q. J.; Chan-Park, M. B.; Zhuo, Q.; Lu, Z. S.; Li, C. M.; Ong, B. S. *Org. Electron.* **2008**, *9*, 936.

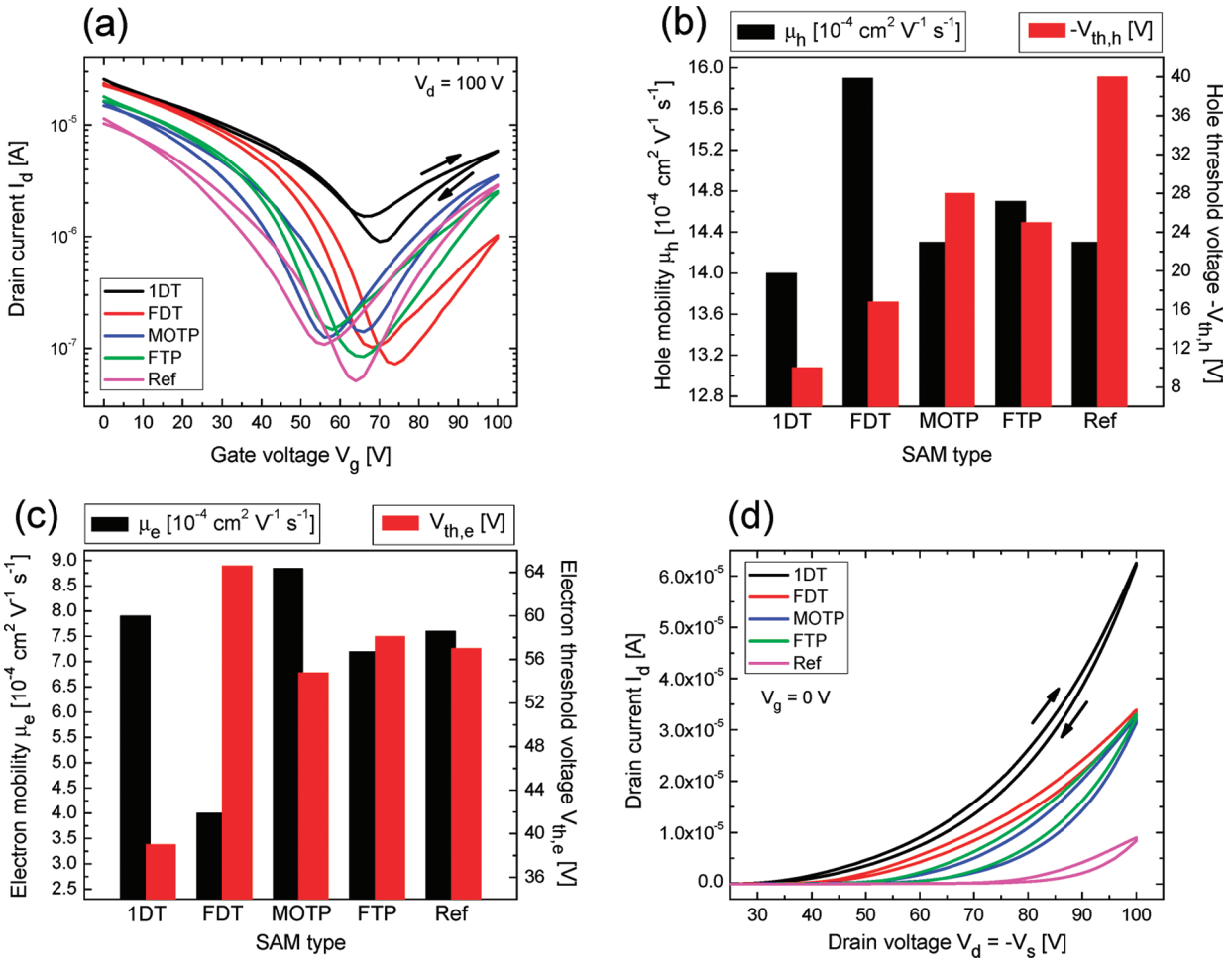

Figure 5. (a) Comparison of the LEFET transfer characteristics for different applied SAMs (1DT, FDT, MOTP, FTP) in comparison to the bare gold reference (Ref) ($L = 10\,\mu$m, $W = 5$ mm, 70 nm F8BT, 390 nm PMMA, 10 nm Ag gate). Graphs (b) and (c) illustrate the extrapolation of the hole and electron mobilities μ and threshold voltages V_{th}, respectively. (d) Transistor current I_d for the different devices during an ambipolar IV-sweep with $V_g = 0$ V and $V_d = -V_s$.

enhance the current in the electron injection regime at the expense of the current in the hole injection regime, whereas SAMs with dipole moment pointing toward the gold electrode like FDT and FTP improve hole injection. The performance behavior of devices with 1DT-modified gold electrodes, however, disagrees strongly with the simple workfunction explanation. While the electron injection is expected to be best in 1DT-based devices, the current in the hole injection regime is also considerably enhanced as a consequence of very low threshold voltages for both charge carriers being observed. Even the hole mobility of 1DT-modified gold electrodes is comparable to that of unmodified gold, and in some cases was even found to be slightly higher than that of unmodified gold.

We have recently undertaken a detailed investigation of the mechanisms, by which SAM modification of gold electrodes, exemplarily using 1DT and FDT, influences ambipolar charge injection.[35] Workfunction modification alone cannot explain the observed improvement of charge injection for both electron and holes simultaneously. One major factor responsible for the good ambipolar charge injection with SAM-modified electrodes was found to be a reduction of the film thickness of a spin-coated polymer film directly on top of SAM-treated gold. As a result of a more hydrophobic surface with lower surface energy compared to bare gold, as quantified by the contact angle measurements in Table 1, a local thickness reduction on top of the electrodes of typically 20−30 nm is observed. [35] As the component of contact resistance due to transport through the bulk before reaching the accumulation layer at the dielectric interface becomes smaller this way,[17] the electron and hole currents are improved. In addition to this effect, the hydrophobic, low surface-tension modification of the gold electrodes with SAMs has also been shown to beneficially affect the interfacial polymer microstructure within the first F8BT layers on top of the electrodes and, generally, the physical contact of the film with the electrodes. [35]

These results shed light on the reasons why high temperature annealing had to be used in previous work on ambipolar F8BT LEFETs[7,9,14] as well as in other studies on unipolar polyfluorene-based FETs[36] to achieve

(35) Cheng, X.; Noh, Y.-Y.; Wang, J.; Tello, M.; Frisch, J.; Blum, R.-P.; Vollmer, A.; Rabe, J. P.; Koch, N.; Sirringhaus, H. *Adv. Funct. Mater.* **2009**, *19*, 2407.

(36) Sirringhaus, H.; Wilson, R. J.; Friend, R. H.; Inbasekaran, M.; Wu, W.; Woo, E. P.; Grell, M.; Bradley, D. D. C. *Appl. Phys. Lett.* **2000**, *77*, 406.

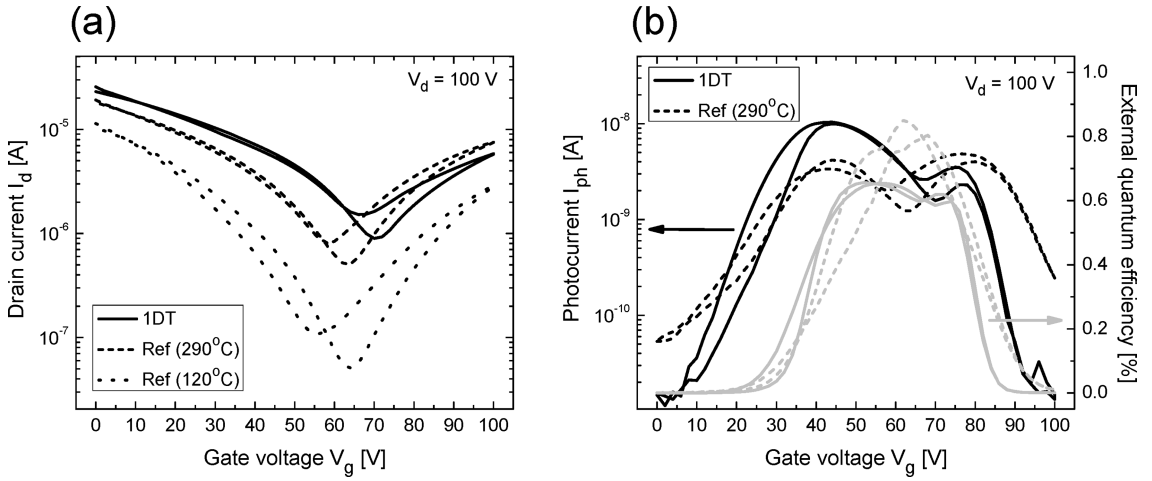

Figure 6. (a) Comparison of the LEFET transfer characteristics for a 1DT-modified device with reference devices annealed at 290 °C and 120 °C (L = 10 μm, W = 5 mm, 70 nm F8BT, 390 nm PMMA, 10 nm Ag gate). (b) Corresponding photocurrents measured with a diode on top of the device and calculated external quantum efficiencies.

optimum device performance. This could in principle be due to a number of possible factors influenced by annealing, such as the need to achieve a favorable polymer microstructure at the active interface with the gate dielectric, elimination of specific structural defects and/or chemical impurities, and/or a general reduction of channel resistance. Our observation here that similarly stable ambipolar device performance can also be achieved by SAM modification of the electrodes without high-temperature annealing of the film indicates, however, that the main requirement for stable ambipolar performance is not the need to improve the electronic properties in the channel but the need to reduce the source−drain contact resistance. If there were traps or impurities in the channel that had to be removed from the as-deposited films to achieve stable ambipolar performance, these would be likely to remain in SAM treated devices not annealed to high temperature and would prevent achieving low threshold voltages and hysteresis. This indicates that the main benefit of the high-temperature annealing might not be improvement of the channel resistance but of the source−drain contact resistance. Of course the mechanism by which annealing lowers the contact resistance is likely to be different from the corresponding mechanism acting in the case of SAM treatment. A detailed understanding of this mechanism goes beyond the scope of this work. We can hypothesize that given the significant changes in film morphology annealing might induce a more favorable interfacial microstructure at the metal−polymer interface or in the bulk of the polymer above the electrodes or it might generally improve the physical contact between the electrode and the polymer film. In any case by SAM modification of the electrodes the need for high-temperature annealing can be effectively eliminated.

The comparison of the ambipolar current characteristics in Figure 4d clearly states that 1DT with the discovered favorable electron and hole transport properties can be used to substantially increase the light emission without losing the amorphous character of the F8BT, which is required for efficient waveguiding and light gain. The transfer characteristics of a 1DT-modified device in Figure 6a confirm that ambipolar current levels can be reached, which are comparable or even higher than those of polycrystalline devices with F8BT annealed at 290 °C. The dramatic performance improvement with more than an order of magnitude larger current in the ambipolar regime becomes obvious by comparing the 1DT-modified device to the unmodified 120 °C reference device. Due to the 1DT, the currents in the hole transport regime become larger, as the mobility decrease from 1.57×10^{-3} cm^2 V^{-1} s^{-1} for a 290 °C device to 1.40×10^{-3} cm^2 V^{-1} s^{-1} is overcompensated by the threshold reduction from −24 V to only −10 V. Despite the still slightly lower current in the pure electron injection regime, caused by a lower mobility of about 8.0×10^{-4} cm^2 V^{-1} s^{-1} instead of 9.6×10^{-4} cm^2 V^{-1} s^{-1} and comparable thresholds of 39 and 36 V, respectively, the current in the crucial ambipolar regime is doubled in the 1DT-modified amorphous device. The resulting photocurrents during the transfer scan are plotted in Figure 6b. They are detected on top of the device through the respective semitransparent 10 nm thick silver gate electrode. In both cases a wide ambipolar regime with intense light emission is observed. As a result of the higher currents in the ambipolar regime, the photocurrent measurement reveals even higher maximum light intensities in the amorphous device with 1DT. Furthermore, with the help of the typical F8BT electroluminescence (EL) spectrum, accessible in the Supporting Information (Figure S5), one is able to extract the external quantum efficiency (EQE), which is also plotted in Figure 6b. The EQE of the 1DT-modified amorphous F8BT device is slightly lower with a peak value of about 0.65% than that of the polycrystalline F8BT device with a maximum EQE of about 0.85%. A slight increase of the PL efficiency of polycrystalline compared to amorphous F8BT could in principle cause a minor EQE difference.[18] However, the different EQE is believed to be due to the morphological difference between the two films in combination with the detection method, in which only the

light that is transmitted through the gate is collected. The emitted light is waveguided within the F8BT slab before out-of-plane scattering induces strong surface emission. This effect, which is particularly considerable for polycrystalline F8BT annealed at 290 °C, is believed to explain the observation of different EQE values, given the strong variations in the ASE performance of F8BT, and emphasizes the importance of amorphous F8BT for in-plane waveguiding and simultaneous gain.

Conclusions

In summary, the LEFET processing and in particular the effects of post-spin-coating annealing, which changes the morphology of an F8BT film, are of crucial importance for efficient light-waveguiding or amplifying applications such as in integrated optoelectronic circuits, waveguides, and lasers. The increasing surface roughness and the progressing crystallization beyond annealing temperatures of 120 °C suppresses ASE behavior due to severe scattering, requiring amorphous F8BT films to be used as the active layer of the LEFET. An efficient way of tuning ambipolar charge carrier injection and improving the interface morphology is to modify the gold electrodes with different types of SAMs. It has been found that the SAM 1-decanethiol enhances the charge injection and thus the current in both charge carrier regimes, which has to be attributed to substantially reduced contact resistance due to a thinner F8BT film on top of the injecting electrodes and hence reduced bulk resistance, as well as a more favorable arrangement of the F8BT directly at the electrode interface, in addition to the modification of the effective electrode workfunction. Using this SAM allows lowering the previously used very high annealing temperatures above the F8BT melting point down to moderate temperatures below the F8BT melting point. As a result, the LEFET currents in the ambipolar regime become even higher than in devices with polycrystalline F8BT, making the 1DT modification an efficient method to enhance the light emission intensity, which is required for low-loss waveguide applications or a possible electrically driven laser.

Acknowledgment. We are thankful to K.K. Banger for help with the DSC measurement as well as J. Nelson and J. Dane for help with the SKPM and contact angle measurements. We acknowledge M. Bird, R.C.G. Naber, and X. Cheng for useful discussions. This work was financially supported by "Deutsche Forschungsgemeinschaft" (DFG Project GI 269/7-1). M.C.G. thanks the "Studienstiftung des Deutschen Volkes" and the "Gates Cambridge Trust" for financial support.

Supporting Information Available: Extrapolated electron/hole mobilities and threshold voltages as a function of F8BT annealing temperature (S1), ASE spectrum and threshold analysis for 120 °C F8BT films (S2), schematic of the energetic influence of an interface dipole induced by a SAM (S3), output characteristics of LEFETs with SAM-modified injecting gold electrodes (S4), and electroluminescence spectrum of F8BT LEFET (S5). This material is available free of charge via the Internet at http://pubs.acs.org.